

## Finite element analysis of 2D turbulent flows using the logarithmic form of the $k$ - $\varepsilon$ model

Hiroshi Hasebe\* and Takashi Nomura

Department of Civil Engineering, CST, Nihon University,  
Kanda-Surugadai 1-8-14, Chiyoda-ku, Tokyo 101-8308, Japan  
(Received May 17, 2007, Accepted November 22, 2008)

**Abstract.** The logarithmic form for turbulent flow analysis guarantees the positivity of the turbulence variables as  $k$  and  $\varepsilon$  of the  $k$ - $\varepsilon$  model by using the natural logarithm of these variables. In the present study, the logarithmic form is incorporated into the finite element solution procedure for the unsteady turbulent flow analysis. A backward facing step flow using the standard  $k$ - $\varepsilon$  model and a flow around a 2D square cylinder using the modified  $k$ - $\varepsilon$  model (the Kato-Launder model) are simulated. These results show that the logarithmic form effectively keeps adequate balance of turbulence variables and makes the analysis stable during transient or unsteady processes.

**Keywords:** logarithmic form;  $k$ - $\varepsilon$  model; finite element method; backward facing step; square-cylinder.

### 1. Introduction

The  $k$ - $\varepsilon$  model is one of the widely-used models to simulate turbulent flows around structures (Lardeau and Leschziner 2005, Yoshie, *et al.* 2007) and over complex terrains (Maurizi, *et al.* 1998, Yamaguchi, *et al.* 2003). There are several types of model, such as the standard  $k$ - $\varepsilon$  model (Launder and Spalding 1974), the low Reynolds-number  $k$ - $\varepsilon$  model (Jones and Launder 1972) and the non-linear  $k$ - $\varepsilon$  model (Craft, *et al.* 1996, Abe, *et al.* 2003). Most of these models consist of four variables, the vector of ensemble-averaged velocity  $\bar{\mathbf{U}}$ , the ensemble-averaged pressure  $\bar{P}$ , the turbulent kinetic energy  $k$  and the turbulent dissipation rate  $\varepsilon$ . The Reynolds stress tensor  $\overline{\mathbf{u}'\mathbf{u}'}$ , which is the correlation of the fluctuating velocity  $\mathbf{u}'$ , is modeled by using the linear or non-linear eddy viscosity concepts. In these models, the eddy viscosity  $\nu_t$  is calculated from  $k$  and  $\varepsilon$ . For instance, in case of the standard linear eddy viscosity model, the eddy viscosity is defined as  $\nu_t = C_\mu k^2/\varepsilon$  where  $C_\mu = 0.09$  is a constant. According to the definition  $k$  and  $\varepsilon$  are positive quantities. However, there are cases that these turbulence variables become negative when undershoot of the solution occurs in the computation. When the turbulent dissipation rate  $\varepsilon$  falls into a small negative value, the eddy viscosity  $\nu_t$  varies from a large positive value to a large negative one drastically since  $\varepsilon$  is the denominator of  $\nu_t$ . Such situation causes instability of the computation.

To circumvent this problem, several approaches such as the clipping and the limiter have been devised

---

\* Corresponding Author, E-mail: [hasebe@civil.cst.nihon-u.ac.jp](mailto:hasebe@civil.cst.nihon-u.ac.jp)

(Ilinca, *et al.* 1998). The clipping is a device which replaces a value of the turbulence variables to an appropriate positive one when it becomes negative. The limiter is a device which corrects a value of the turbulence variables to a pre-assigned small positive value when it becomes less than the tolerance. Both devices make it possible to keep the positivity of these turbulence variables. However, strictly speaking, they are meaningless from the physical point of view, and they violate the conservative law.

Ilinca, *et al.* (1998) insist the shortcomings of clipping and limiter, that is, they cause noises and oscillation in the solution field, and make the convergence of iteration solver slow or destroy the calculation. Thus, they proposed the logarithmic form to avoid using clipping and limiter (Ilinca and Pelletier 1998).

The logarithmic form is applied to the  $k$ - $\varepsilon$  model as follows: firstly, new variables  $K$  and  $E$  which are the natural logarithm of  $k$  and  $\varepsilon$  are introduced as  $K = \ln k$  and  $E = \ln \varepsilon$ . Secondly, the transport equations of  $K$  and  $E$  are derived. Finally, these new equations are solved instead of the  $k$  and  $\varepsilon$  equations and the value of the original variables  $k$  and  $\varepsilon$  are recovered by using the exponential functions,  $k = e^K$  and  $\varepsilon = e^E$ . In the logarithmic form, the use of the exponential function to recover the original variables guarantees the positivity of them. Therefore, the logarithmic form prevents negative eddy viscosity without any numerical technique.

Ilinca and Pelletier (1998) applied the logarithmic form to the adaptive remeshing analysis based on the minimum residual by using the steady  $k$ - $\varepsilon$  model and this work was followed by Ignat, *et al.* (2000), Turgeon, *et al.* (2000) and Lacasse, *et al.* (2001). In the adaptive remeshing analysis large gradients and deviations of curvature in the solution field should be avoided because they disturb the convergence of the iteration solver.

Luo, *et al.* (2003) applied the logarithmic form to the computation of compressible flows. In their paper, they stated that the effect of the use of the logarithmic form can alleviate the stiffness of the turbulent equations.

Although these studies discuss the effects of the logarithmic form with respect to the convergence of the iterative solver and the mesh refinement, they do not mention to the transient process and the flow around bluff body with vortex sheddings. In this paper, we incorporated the logarithmic form into the finite element solution procedure for the unsteady turbulent flow analysis. We calculated a backward facing step flow and a flow around a 2D square cylinder. From these results, we discuss the effect of the logarithmic form to the transient process as well as the flow around bluff body.

## 2. Governing equation

The  $k$ - $\varepsilon$  model which is used in this paper consists of the Reynolds Averaged Navier-Stokes equation [Eq. (1)] and the continuity equation [Eq. (2)] as described below:

$$\rho \left( \frac{\partial \bar{\mathbf{U}}}{\partial t} + \bar{\mathbf{U}} \cdot \nabla \bar{\mathbf{U}} - \bar{\mathbf{f}} \right) - \nabla \cdot (\bar{\boldsymbol{\sigma}} - \rho \overline{\mathbf{u}'\mathbf{u}'} ) = \mathbf{0} \quad \text{in } \Omega, \quad (1)$$

$$\nabla \cdot \bar{\mathbf{U}} = 0 \quad \text{in } \Omega. \quad (2)$$

In Eqs. (1) and (2),  $\Omega$  is the computational domain with the boundary  $\Gamma$ ,  $\bar{\mathbf{U}}$  is the vector of ensemble-averaged velocity,  $\bar{\mathbf{f}}$  is the force vector,  $\bar{\boldsymbol{\sigma}}$  is the stress tensor which is defined as follows:

$$\bar{\boldsymbol{\sigma}} = -\bar{P}\mathbf{I} + 2\mu s(\bar{\mathbf{U}}), \quad (3)$$

with

$$s(\bar{\mathbf{U}}) = \frac{1}{2} \{ \nabla \bar{\mathbf{U}} + (\nabla \bar{\mathbf{U}})^T \}. \quad (4)$$

$\bar{P}$  is the ensemble-averaged pressure,  $\rho$  is the density,  $\mu$  is the viscosity,  $\mathbf{I}$  is the identity tensor. The term  $\rho \overline{\mathbf{u}'\mathbf{u}'}$ , the Reynolds stresses, is modeled in the  $k$ - $\varepsilon$  models as follows:

$$-\rho \overline{\mathbf{u}'\mathbf{u}'} = 2\mu_t s(\bar{\mathbf{U}}) - \frac{2}{3} \rho k \mathbf{I}, \quad (5)$$

with

$$\mu_t = \rho \nu_t = \rho C_\mu \frac{k^2}{\varepsilon}, \quad (6)$$

where  $\mu_t$  is the turbulent viscosity,  $\nu_t$  is the eddy viscosity (or the turbulent kinematic viscosity),  $k$  is the turbulent kinetic energy,  $\varepsilon$  is the turbulent dissipation rate and  $C_\mu$  is a constant.

The transport equations for  $k$  and  $\varepsilon$  are described as follows:

$$\frac{\partial k}{\partial t} + \bar{\mathbf{U}} \cdot \nabla k = \nabla \cdot \left[ \left( \mathbf{v} + \frac{\mathbf{v}_t}{\sigma_k} \right) \nabla k \right] + P_k - \varepsilon \quad \text{in } \Omega, \quad (7)$$

$$\frac{\partial \varepsilon}{\partial t} + \bar{\mathbf{U}} \cdot \nabla \varepsilon = \nabla \cdot \left[ \left( \mathbf{v} + \frac{\mathbf{v}_t}{\sigma_\varepsilon} \right) \nabla \varepsilon \right] + \frac{\varepsilon}{k} (C_{\varepsilon 1} P_k - C_{\varepsilon 2} \varepsilon) \quad \text{in } \Omega, \quad (8)$$

where the standard values of the model constants appearing in Eqs. (6), (7) and (8) are:

$$C_\mu = 0.09, C_{\varepsilon 1} = 1.44, C_{\varepsilon 2} = 1.92, \sigma_k = 1.0, \sigma_\varepsilon = 1.3. \quad (9)$$

In Eqs. (7) and (8),  $P_k$  is the production term. In the case of the standard  $k$ - $\varepsilon$  model and the Kato-Launder model (1997), both of which are employed below in this paper, the production term is defined as follows:

$$P_k = C_\mu \varepsilon \hat{S}^2 \quad (\text{the standard } k\text{-}\varepsilon \text{ model}), \quad (10)$$

$$P_k = C_\mu \varepsilon \hat{S} \hat{\Omega} \quad (\text{the Kato-Launder model}), \quad (11)$$

where

$$\hat{S} = \frac{k}{\varepsilon} \sqrt{\frac{1}{2} (\nabla \bar{\mathbf{U}} + \nabla \bar{\mathbf{U}}^T)^2}, \quad \hat{\Omega} = \frac{k}{\varepsilon} \sqrt{\frac{1}{2} (\nabla \bar{\mathbf{U}} - \nabla \bar{\mathbf{U}}^T)^2}. \quad (12), (13)$$

On the boundary  $\Gamma$  of the computational domain  $\Omega$ , the following boundary conditions can be imposed at different segments of the boundary  $\Gamma$ :

$$\bar{\mathbf{U}} = \mathbf{g}_{\bar{\mathbf{U}}}, \quad k = g_k, \quad \varepsilon = g_\varepsilon \quad \text{on } \Gamma_g, \quad (14a, b, c)$$

$$(\bar{\boldsymbol{\sigma}} - \rho \overline{\mathbf{u}'\mathbf{u}'} ) \mathbf{n} = \mathbf{h}_{\bar{\mathbf{U}}}, \quad \left( \mathbf{v} + \frac{\mathbf{v}_t}{\sigma_k} \right) \nabla k \cdot \mathbf{n} = h_k, \quad \left( \mathbf{v} + \frac{\mathbf{v}_t}{\sigma_\varepsilon} \right) \nabla \varepsilon \cdot \mathbf{n} = h_\varepsilon \quad \text{on } \Gamma_h, \quad (15a, b, c)$$

where  $\mathbf{g}_{\bar{\mathbf{U}}}$ ,  $g_k$ ,  $g_\varepsilon$ ,  $\mathbf{h}_{\bar{\mathbf{U}}}$ ,  $h_k$  and  $h_\varepsilon$  are the prescribed values, and  $\mathbf{n}$  is the unit outward normal vector on  $\Gamma$ .

### 3. Logarithmic form

According to the physical meanings and the definition, both the turbulent kinetic energy  $k$  and the turbulent dissipation rate  $\varepsilon$  are positive quantities. However, the positivity may not be guaranteed in the computation. Ilinca and Pelletier (1998) proposed the logarithmic form to guarantee the positivity of the turbulence variables mathematically.

The logarithmic form employs new variables which are the natural logarithm of the original turbulence variables. In the case of the  $k$ - $\varepsilon$  model, the new variables are defined as:

$$K \equiv \ln k, \quad E \equiv \ln \varepsilon, \quad (16a, b)$$

where  $K$  is the natural logarithm of  $k$  and  $E$  is that of  $\varepsilon$ .

To derive the transport equations for  $K$  and  $E$  from the original equations [Eqs. (7) and (8)], the following differential relations are applied.

$$\frac{\partial K}{\partial t} = \frac{1}{k} \frac{\partial k}{\partial t}, \quad \nabla K = \frac{1}{k} \nabla k, \quad (17a, b)$$

$$\frac{\partial E}{\partial t} = \frac{1}{\varepsilon} \frac{\partial \varepsilon}{\partial t}, \quad \nabla E = \frac{1}{\varepsilon} \nabla \varepsilon. \quad (18a, b)$$

After dividing Eq. (7) by  $k$  and Eq. (8) by  $\varepsilon$ , the application of Eq. (17a, b) and Eq. (18a, b) leads to the transport equations for  $K$  and  $E$ :

$$\frac{\partial K}{\partial t} + \bar{\mathbf{U}} \cdot \nabla K = \nabla \cdot \left[ \left( \mathbf{v} + \frac{\mathbf{v}_t}{\sigma_k} \right) \nabla K \right] + \left( \mathbf{v} + \frac{\mathbf{v}_t}{\sigma_k} \right) (\nabla K)^2 + e^{-K} P_k - \frac{C_\mu}{v_t} e^K \quad \text{in } \Omega, \quad (19)$$

$$\frac{\partial E}{\partial t} + \bar{\mathbf{U}} \cdot \nabla E = \nabla \cdot \left[ \left( \mathbf{v} + \frac{\mathbf{v}_t}{\sigma_\varepsilon} \right) \nabla E \right] + \left( \mathbf{v} + \frac{\mathbf{v}_t}{\sigma_\varepsilon} \right) (\nabla E)^2 + C_{\varepsilon 1} e^{-K} P_k - C_{\varepsilon 2} e^{E-K} \quad \text{in } \Omega, \quad (20)$$

where the last term in Eq. (19) is rewritten by using the following eddy viscosity relation:

$$e^E = \frac{C_\mu}{v_t} e^{2K}. \quad (21)$$

The boundary conditions of the new variables,  $K$  and  $E$ , can be described as:

$$K = g_K, \quad E = g_E \quad \text{on } \Gamma_g, \quad (22a, b)$$

$$\left( \mathbf{v} + \frac{\mathbf{v}_t}{\sigma_k} \right) \nabla K \cdot \mathbf{n} = h_K, \quad \left( \mathbf{v} + \frac{\mathbf{v}_t}{\sigma_\varepsilon} \right) \nabla E \cdot \mathbf{n} = h_E \quad \text{on } \Gamma_h, \quad (23a, b)$$

where  $g_K$ ,  $g_E$ ,  $h_K$  and  $h_E$  are the following prescribed values:

$$g_K \equiv \ln g_k, \quad g_E \equiv \ln g_\varepsilon, \quad (24a, b)$$

$$h_K \equiv \frac{1}{k} h_k, \quad h_E \equiv \frac{1}{\varepsilon} h_\varepsilon. \quad (25a, b)$$

The second terms of the R.H.S. in Eqs. (19) and (20), the square of the gradient, are called “the second diffusion term”. The presence of the second diffusion terms is the greatest difference between the equations using the logarithmic variables and the original ones. In the followings, we

call the  $k$ - $\varepsilon$  model described in terms of the original variables as “the normal form”.

#### 4. Finite element method

The computational domain  $\Omega$  is subdivided into the finite elements  $\Omega^e$ ,  $e = 1, 2, \dots, N_{el}$ , where  $N_{el}$  is the number of elements. Then the SUPG stabilized finite element formulation of Eqs. (1), (2), (19) and (20) can be written as follows:

[Momentum equation]

$$\begin{aligned} & \int_{\Omega} \mathbf{w}_{\bar{\mathbf{u}}}^h \cdot \left\{ \rho \left( \frac{\partial \bar{\mathbf{u}}^h}{\partial t} + \bar{\mathbf{u}}^h \cdot \nabla \bar{\mathbf{u}}^h - \bar{\mathbf{f}}^h \right) \right\} d\Omega + \int_{\Omega} s(\mathbf{w}_{\bar{\mathbf{u}}}^h) : (\bar{\boldsymbol{\sigma}}^h - \rho \overline{\mathbf{u}'^h \mathbf{u}'^h}) d\Omega \\ & + \sum_{e=1}^{N_{el}} \left[ \int_{\Omega^e} \tau_{\bar{\mathbf{u}}} \bar{\mathbf{u}}^h \cdot \nabla \mathbf{w}_{\bar{\mathbf{u}}}^h \cdot \left\{ \rho \left( \frac{\partial \bar{\mathbf{u}}^h}{\partial t} + \bar{\mathbf{u}}^h \cdot \nabla \bar{\mathbf{u}}^h - \bar{\mathbf{f}}^h \right) - \nabla \cdot (\bar{\boldsymbol{\sigma}}^h - \rho \overline{\mathbf{u}'^h \mathbf{u}'^h}) \right\} d\Omega \right] \\ & = \int_{\Gamma_h} \mathbf{w}_{\bar{\mathbf{u}}}^h \cdot \mathbf{h}_{\bar{\mathbf{u}}}^h d\Gamma. \end{aligned} \quad (26)$$

[Continuity equation]

$$\int_{\Omega} q^h (\nabla \cdot \bar{\mathbf{u}}^h) d\Omega = 0. \quad (27)$$

[ $K$  equation ( $K = \ln k$ )]

$$\begin{aligned} & \int_{\Omega} w_K^h \left\{ \frac{\partial K^h}{\partial t} + \bar{\mathbf{u}}^h \cdot \nabla K^h - (\nabla K^h)^2 \right\} d\Omega + \int_{\Omega} \nabla w_K^h \cdot \left( \mathbf{v} + \frac{\mathbf{v}_t^h}{\sigma_k} \right) \nabla K^h d\Omega \\ & + \sum_{e=1}^{N_{el}} \left[ \int_{\Omega^e} \tau_K \bar{\mathbf{u}}^h \cdot \nabla w_K^h \left\{ \frac{\partial K^h}{\partial t} + \bar{\mathbf{u}}^h \cdot \nabla K^h - \nabla \cdot \left( \mathbf{v} + \frac{\mathbf{v}_t^h}{\sigma_k} \right) \nabla K^h - (\nabla K^h)^2 - e^{-K^h} P_k^h + \frac{C_{\mu}}{v_t^h} e^{K^h} \right\} d\Omega \right] \\ & = \int_{\Omega} w_K^h \left( e^{-K^h} P_k^h - \frac{C_{\mu}}{v_t^h} e^{K^h} \right) d\Omega + \int_{\Gamma_h} w_K^h h_K^h d\Gamma. \end{aligned} \quad (28)$$

[ $E$  equation ( $E = \ln \varepsilon$ )]

$$\begin{aligned} & \int_{\Omega} w_E^h \left\{ \frac{\partial E^h}{\partial t} + \bar{\mathbf{u}}^h \cdot \nabla E^h - (\nabla E^h)^2 \right\} d\Omega + \int_{\Omega} \nabla w_E^h \cdot \left( \mathbf{v} + \frac{\mathbf{v}_t^h}{\sigma_{\varepsilon}} \right) \nabla E^h d\Omega \\ & + \sum_{e=1}^{N_{el}} \left[ \int_{\Omega^e} \tau_E \bar{\mathbf{u}}^h \cdot \nabla w_E^h \left\{ \frac{\partial E^h}{\partial t} + \bar{\mathbf{u}}^h \cdot \nabla E^h - \nabla \cdot \left( \mathbf{v} + \frac{\mathbf{v}_t^h}{\sigma_{\varepsilon}} \right) \nabla E^h - (\nabla E^h)^2 - C_{\varepsilon 1} e^{-K^h} P_k^h + C_{\varepsilon 2} e^{E^h - K^h} \right\} d\Omega \right] \\ & = \int_{\Omega} w_E^h (C_{\varepsilon 1} e^{-K^h} P_k^h + C_{\varepsilon 2} e^{E^h - K^h}) d\Omega + \int_{\Gamma_h} w_E^h h_E^h d\Gamma, \end{aligned} \quad (29)$$

where  $\mathbf{w}_{\bar{U}}^h$ ,  $q^h$ ,  $w_k^h$  and  $w_E^h$  are the weighting functions.

In this paper, Q1P0 elements are employed, where the trial solutions and weighting functions described above are defined in each element as follows:

$$\begin{aligned}\bar{\mathbf{U}}^h &= \mathbf{N}_{\bar{U}} \bar{\mathbf{U}}^e, \quad \bar{P}^h = N_{\bar{P}} \bar{P}^e, \quad K^h = \mathbf{N}_K \mathbf{K}^e, \quad E^h = \mathbf{N}_E \mathbf{E}^e, \\ \mathbf{w}_{\bar{U}}^h &= \mathbf{N}_{\bar{U}} \mathbf{w}_{\bar{U}}^e, \quad q^h = N_{\bar{P}} q^e, \quad w_k^h = \mathbf{N}_K \mathbf{w}_K^e, \quad w_E^h = \mathbf{N}_E \mathbf{w}_E^e,\end{aligned}\quad (30a\sim h)$$

where  $\mathbf{N}_{\bar{U}}$  is the matrix of the bilinear shape functions,  $\mathbf{N}_K$  and  $\mathbf{N}_E$  are the vectors of the bilinear shape functions,  $N_{\bar{P}}$  is the piecewise constant shape function.  $\bar{\mathbf{U}}^e$ ,  $\mathbf{K}^e$  and  $\mathbf{E}^e$  are the elementwise local nodal value vectors,  $\bar{P}^e$  is the piecewise constant pressure in the element.  $\mathbf{w}_{\bar{U}}^e$ ,  $\mathbf{w}_K^e$  and  $\mathbf{w}_E^e$  are the vectors of the elementwise weighting functions,  $q^e$  is the piecewise constant weighting function for the continuity equation.  $\tau_{\bar{U}}$ ,  $\tau_K$  and  $\tau_E$  are the SUPG stabilization parameters calculated as follows:

$$\tau_{\phi} = \frac{\xi_{\phi} \bar{U}_{\xi} h_{\xi} + \eta_{\phi} \bar{U}_{\eta} h_{\eta}}{2(\bar{U}^2 + \bar{V}^2)}, \quad (31)$$

where  $\phi$  corresponds to  $\bar{U}$ ,  $K$  or  $E$ .  $\bar{U}_{\xi}$  and  $\bar{U}_{\eta}$  are the component of the velocity vector evaluated at the center of the elements.  $h_{\xi}$  and  $h_{\eta}$  are the element length on the local coordinates  $\xi$  and  $\eta$ . Fig. 1 shows the definition of the  $\bar{U}_{\xi}$ ,  $\bar{U}_{\eta}$ ,  $h_{\xi}$  and  $h_{\eta}$ . The parameters  $\xi_{\phi}$  and  $\eta_{\phi}$  in Eq. (31) are calculated as follows:

$$\xi_{\phi} = \frac{1}{\alpha_{\xi\phi}} - \coth \alpha_{\xi\phi}, \quad \eta_{\phi} = \frac{1}{\alpha_{\eta\phi}} - \coth \alpha_{\eta\phi}, \quad (32a, b)$$

$$\alpha_{\xi\phi} = \frac{\bar{U}_{\xi} h_{\xi}}{2k_{\phi}}, \quad \alpha_{\eta\phi} = \frac{\bar{U}_{\eta} h_{\eta}}{2k_{\phi}}, \quad (33a, b)$$

where  $k_{\phi}$  is the diffusivity of equations.  $\alpha_{\xi\phi}$  and  $\alpha_{\eta\phi}$  are the element peclet number.

Substituting Eqs.(30a~h) into Eqs.(26), (27), (28) and (29), the following matrix form of the finite element equations are obtained.

[Momentum equation]

$$[\mathbf{M} + \tilde{\mathbf{M}}] \dot{\mathbf{u}} + [\mathbf{A} + \tilde{\mathbf{A}}] \mathbf{u} + \mathbf{D} \mathbf{u} - \mathbf{G} \mathbf{p} = \mathbf{f} + \tilde{\mathbf{f}}. \quad (34)$$

[Continuity equation]

$$\mathbf{G}^T \mathbf{u} = \mathbf{0}. \quad (35)$$

[K equation ( $K = \ln k$ )]

$$[\mathbf{M}_K + \tilde{\mathbf{M}}_K] \dot{\mathbf{K}} + [\mathbf{A}_K + \tilde{\mathbf{A}}_K] \mathbf{K} + [\mathbf{D}_K - \mathbf{D}'_K - \tilde{\mathbf{D}}'_K] \mathbf{K} = \mathbf{S}_K + \tilde{\mathbf{S}}_K. \quad (36)$$

[E equation ( $E = \ln \varepsilon$ )]

$$[\mathbf{M}_E + \tilde{\mathbf{M}}_E] \dot{\mathbf{E}} + [\mathbf{A}_E + \tilde{\mathbf{A}}_E] \mathbf{E} + [\mathbf{D}_E - \mathbf{D}'_E - \tilde{\mathbf{D}}'_E] \mathbf{E} = \mathbf{S}_E + \tilde{\mathbf{S}}_E, \quad (37)$$

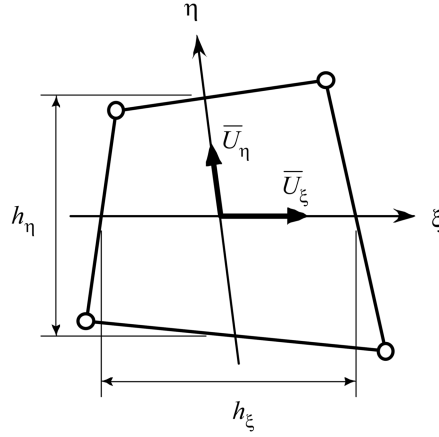


Fig. 1 Definition of local coordinate for estimating the SUPG parameter for the bilinear quadrilateral element

where  $\mathbf{u}$ ,  $\mathbf{K}$  and  $\mathbf{E}$  are the global vector of nodal values. The definitions of their vectors and matrices are given in Appendix A. These equations are solved by the predictor-corrector method (Brooks and Hughes 1982). The details of the time integration loop are shown in Appendix B.

## 5. Wall boundary conditions

We adopted the wall function to the boundary condition on solid boundaries (Mohammadi and Pironneau 1994, Mohammadi and Puigt 2006). Specifically, the wall shear stress is used as the boundary condition. Fig. 2 shows the location of computational solid boundaries and the definition of variables to evaluate the wall shear stress when the wall function is used. In the finite element analysis, the computational solid boundaries are located at the distance  $\delta_w$  away from the actual solid boundary (Lacasse, *et al.* 2004). To evaluate the wall shear stress  $\tau_w$ , we refer to the tangential component of velocity  $\bar{U}_{ref}$  and the turbulent kinetic energy  $k_p$  at the computational boundary nodes. The wall shear stress  $\tau_w$  is defined as follows:

$$\tau_w = -\frac{\rho C_\mu^{1/4} k_p^{1/2}}{\frac{1}{\kappa} \ln(C_E y^+)} \cdot \bar{U}_{ref} \quad (y^+ \geq y_c^+), \quad (38)$$

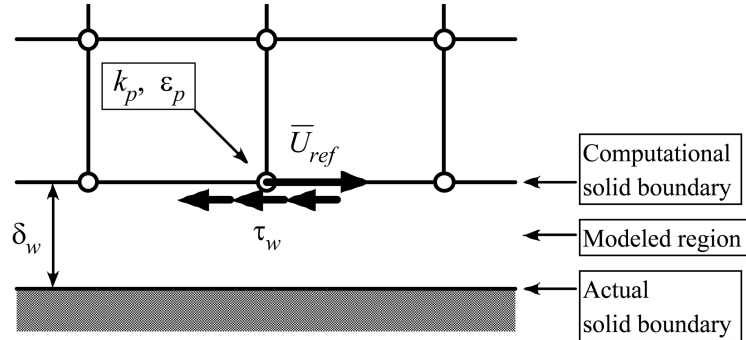


Fig. 2 Definition of variables to determine the wall shear stress

$$\tau_w = -\mu \frac{\bar{U}_{ref}}{\delta_w} \quad (y^+ < y_c^+), \quad (39)$$

where

$$y^+ = C_\mu^{1/4} k_p^{1/2} \delta_w / \nu, \quad (40)$$

is the nondimensional distance from the wall. Then, the equivalent nodal forces of the wall shear stress  $\tau_w$  are used as the boundary condition for the momentum equation [Eq. (1)].  $\kappa$  ( $= 0.4187$ ) is the von Karman constant and  $C_E$  ( $= 9.793$ ) is the roughness parameter.  $y_c^+$  indicates the border between the logarithmic region and the viscous sublayer, which is set as 11.63.

According to Launder and Spalding (1974), to incorporate the effect of the wall shear stress at the wall boundary nodes, the production term  $P_k$  and the dissipation term  $\varepsilon$  in the  $k$  equation [Eq. (7)] are rewritten as follows:

$$P_k = \nu_t \frac{\partial \bar{U}}{\partial y} \cdot \frac{\partial \bar{U}}{\partial y} = \frac{\tau_w}{\rho} \cdot \frac{\bar{U}_{ref}}{\delta_w}, \quad (41)$$

$$\varepsilon = \frac{k^{3/2}}{l} = \frac{k^{3/2}}{\frac{\nu_t}{C_\mu k^{1/2}}} \cdot \frac{\frac{\partial \bar{U}}{\partial y}}{\frac{\partial \bar{U}}{\partial y}} = \frac{\rho C_\mu k_p^2}{\tau_w} \cdot \frac{\bar{U}_{ref}}{\delta_w}. \quad (42)$$

Therefore, the production term  $e^{-K} P_k$  and the dissipation term  $C_\mu e^K / \nu_t$  in the  $K$ -equation [Eq. (19)] are also rewritten as follows:

$$e^{-K} P_k = \frac{1}{k_p} \cdot \frac{\tau_w}{\rho} \cdot \frac{\bar{U}_{ref}}{\delta_w}, \quad (43)$$

$$\frac{C_\mu}{\nu_t} e^K = e^{E-K} = \frac{\rho C_\mu k_p}{\tau_w} \cdot \frac{\bar{U}_{ref}}{\delta_w}. \quad (44)$$

In the  $E$ -equation [Eq. (20)], the value of  $E$  at the wall boundary nodes is given by the following relation:

$$E_p = \ln \varepsilon_p = \ln \left( \frac{C_\mu^{3/4} k_p^{3/2}}{\kappa \delta_w} \right). \quad (45)$$

## 6. Flow over a backward facing step

### 6.1. Computational conditions

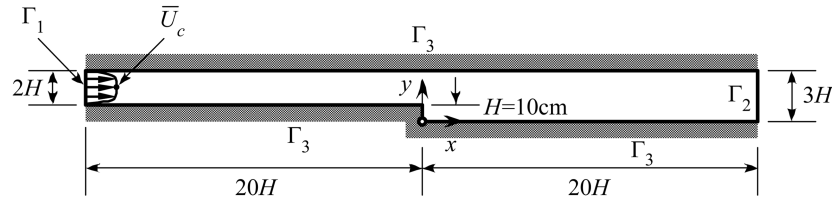
The problem of flow over a backward facing step has served as a benchmark test for turbulent flow simulation in which the reattachment length is the primary concern to be compared (Le, *et al.* 1997, Bauer, *et al.* 2000). We employed the standard  $k$ - $\varepsilon$  model to this problem and compared the result using the logarithmic form with the normal form. The result was also compared to the experimental study by Kasagi, *et al.* (1994).



Fig. 3 shows the computational domain and boundary conditions. Fig. 4 shows the computational mesh around the step. The origin of the horizontal ( $x$ ) and the vertical ( $y$ ) coordinates is taken at the bottom corner of the step in order to describe the reattachment point and other characteristics of the computational results. The number of nodes is 4,719 and the number of elements is 4,502. The Reynolds number  $Re_H$  which is based on the velocity  $\bar{U}_c$  at the center of the inflow boundary and the step height  $H$  is 5,500. The wall function is applied to the upper and lower boundaries  $\Gamma_3$ . The thickness of the modeled region by the wall function  $\delta_w$  is set to  $0.03H$ . For the normal form, we adopted clipping to prevent the negative values and set the clipping values as  $k_c = 1.01\text{cm}^2/\text{s}^2$  and  $\varepsilon_c = 1.01\text{cm}^2/\text{s}^3$ . On the inlet boundary, the turbulent kinetic energy  $k$  and the turbulent dissipation rate  $\varepsilon$  are specified by the following equations:  $k_{in} = (I_u \cdot \bar{U}_{in})^2$ , where  $I_u$  is the turbulent intensity;  $\varepsilon_{in} = k_{in}^{3/2} / \ell$ , where  $\ell$  is the turbulent length scale. In this computation the turbulent intensity  $I_u$  and the turbulent length scale  $\ell$  are set to 2% and 37.88cm, respectively.

## 6.2. Comparison of the reattachment length

Figs. 5 and 6 show the streamlines at the steady state. Fig. 5 is the result of the normal form and Fig. 6 is that of the logarithmic form. Table 1 shows the comparison of the reattachment lengths between the



$\Gamma_1$  :  $\bar{U}_{in}$  = Experimental result by Kasagi, *et al.*

$$k_{in} = (I_u \cdot \bar{U}_{in})^2, \quad \varepsilon_{in} = k_{in}^{3/2} / \ell$$

$$I_u = 2\%, \quad \ell = 37.88\text{cm}$$

$$(\bar{U}_c = 80.37\text{cm/s} : \text{Streamwise velocity component at the center of } \Gamma_1)$$

$\Gamma_2$  :  $\mathbf{h}_{\bar{U}} = h_K = h_E = 0$

$\Gamma_3$  : wall function ( $\delta_w = 0.03H$ )

Fig. 3 Computational domain and boundary conditions

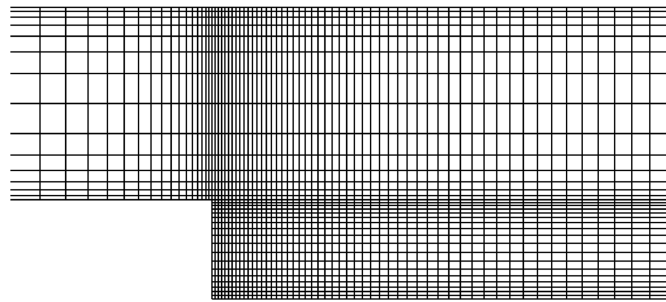


Fig. 4 Computational mesh around the step

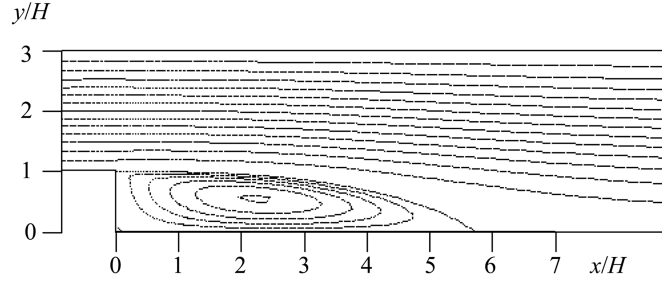


Fig. 5 Streamlines by the normal form

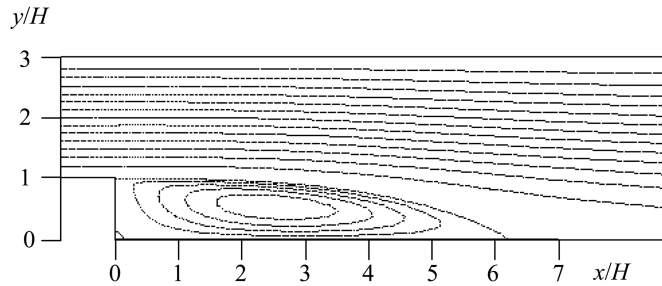


Fig. 6 Streamlines by the logarithmic form

Table 1 Comparison of reattachment lengths

	Normal form	Logarithmic form	Kasagi, <i>et al.</i> (Exp.)
$x/H$	5.7	6.1	6.5

normal form, the logarithmic form and the experimental result by Kasagi, *et al.* (1994). The computational results are both shorter than the experimental one. Figs. 7 and 8 show the distributions of the streamwise mean velocity and the turbulent kinetic energy at 10 sections behind the step. Fig. 7 shows that the distributions of the velocity of the present results are in good agreement with the experimental result. Fig. 8 shows that, except the recirculation region, the turbulent energy distributions are also in good agreement with the experimental result. According to Ferziger (Ferziger, *et al.* 1990), the use of the standard  $k$ - $\epsilon$  model estimates the reattachment length 15% shorter than the experimental one. Therefore, these computational results are reasonable. If we still want to improve the reattachment length, we may employ the low Reynolds-number  $k$ - $\epsilon$  model such as the computational work by Abe, *et al.* (1992) instead of the wall function. However, the objective of the present study is to investigate the effect of the logarithmic form. For this purpose, the present computational results seem to be sufficient.

Although there was no significant difference in the steady results between the normal form and the logarithmic form, the effect of the logarithmic form appeared clearly during the transient process. This difference during transient process will be described and discussed in next section.

### 6.3. Effects of the logarithmic form

At the steady state, there is no significant difference between the logarithmic form and the normal form. However, there is considerable difference in the transient processes, especially in the

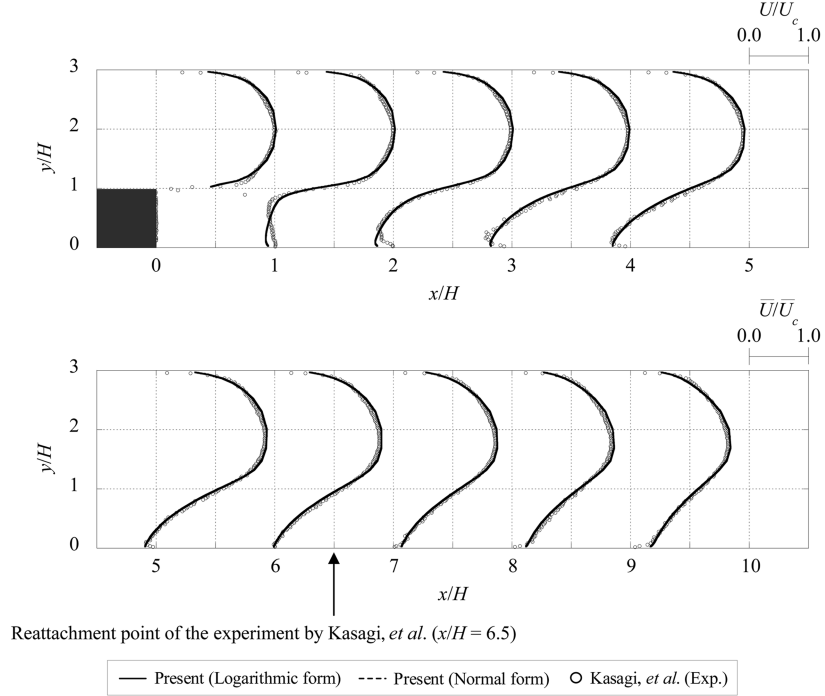


Fig. 7 Distribution of the streamwise mean velocity

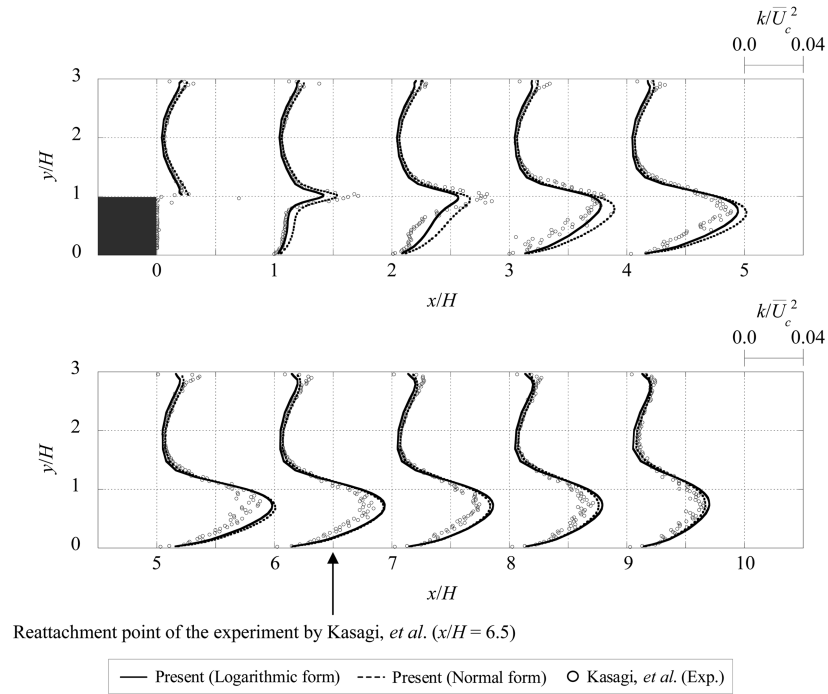


Fig. 8 Distribution of the turbulent kinetic energy

beginning of the computation before the steady state is reached at approximately  $t = 4.0$ s.

Figs. 9 and 10 show the distributions of the eddy viscosity  $\nu_t$  by the normal form and the logarithmic form at the time instants  $t = 1.0$ s,  $2.0$ s and  $3.0$ s. The interval of contour lines is  $5\text{cm}^2/\text{s}$ . The maximum value of the logarithmic form, indicated in Fig. 10 is about  $20\text{cm}^2/\text{s}$ , while, as indicated in Fig. 9, those of the normal form are more than ten times larger than those of the logarithmic form.

Figs. 11 and 12 show the distributions of the turbulent kinetic energy  $k$ , the turbulent dissipation rate  $\varepsilon$  and the eddy viscosity  $\nu_t$  along the broken lines indicated in Figs. 9 (b) and 10 (b). We plotted  $k$  and  $\varepsilon$  in the logarithmic scale. As shown in Fig. 11, for the normal form, the eddy viscosity  $\nu_t$  is extraordinary large around  $x/H = 12$ . In accordance to this, the turbulent dissipation rate  $\varepsilon$  is quite small in this region. The turbulent kinetic energy  $k$  and the turbulent dissipation rate  $\varepsilon$  must maintain a balance such that if  $k$  is large then  $\varepsilon$  is also large. However, this balance between  $k$  and  $\varepsilon$  is not preserved in the normal form. On the contrary as shown in Fig. 12, the balance between  $k$  and  $\varepsilon$  is maintained in the logarithmic form. As the consequence of the definition of Eq. (6), there is no locally excessive eddy viscosity.

Figs. 13 and 14 show the nodal points where clipping occurs to  $k$  and  $\varepsilon$  during the periods from  $0.0$ s to  $1.0$ s,  $1.0$ s to  $2.0$ s and  $2.0$ s to  $3.0$ s. According to Fig. 13(a), clipping to  $k$  mainly occurred

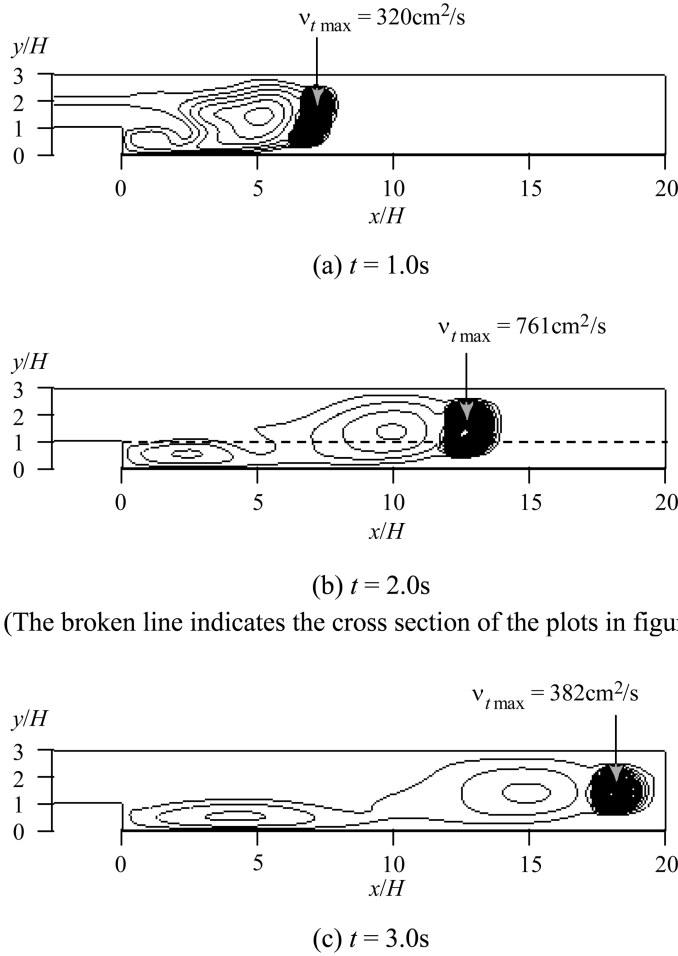
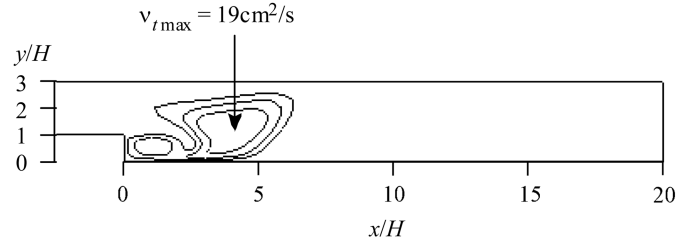
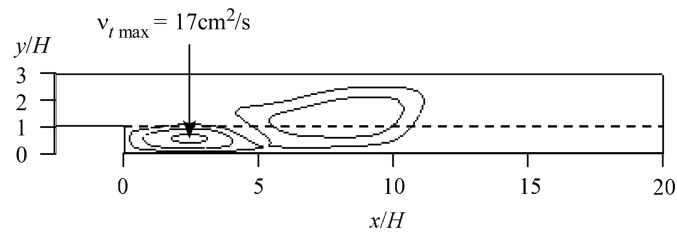


Fig. 9 Distributions of the eddy viscosity by the normal form

(a)  $t = 1.0\text{s}$ (b)  $t = 2.0\text{s}$ 

(The broken line indicates the cross section of the plots in figure 12)

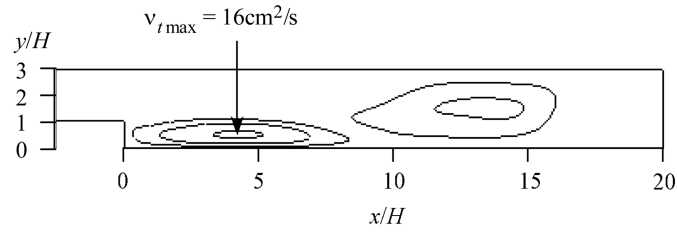
(c)  $t = 3.0\text{s}$ 

Fig. 10 Distributions of the eddy viscosity by the logarithmic form

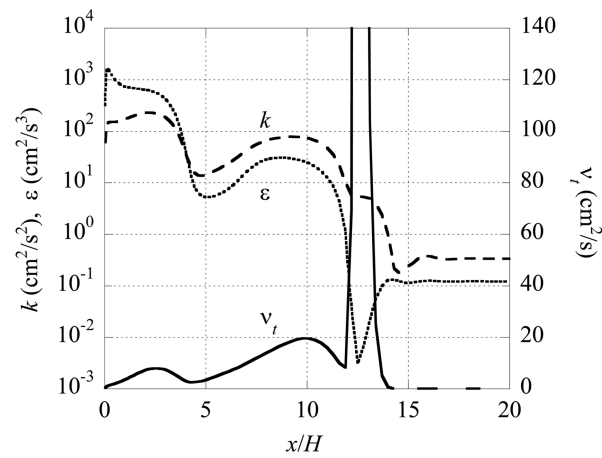


Fig. 11 Distribution of turbulent variables along the broken line in Fig. 9 (b) (the result by the normal form)

behind the step. In this area, the maximum number of clipping to  $k$  was seventeen times per node. According to Fig. 14(a), clipping to  $\varepsilon$  occurred intensively around the step. In this area, the

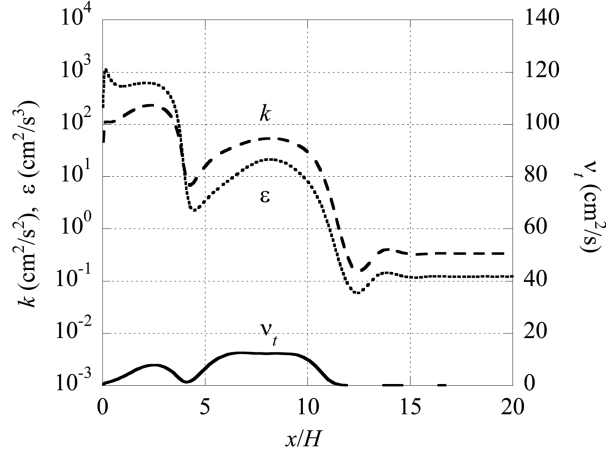


Fig. 12 Distribution of turbulent variables along the broken line in Fig. 10 (b) (the result by the logarithmic form)

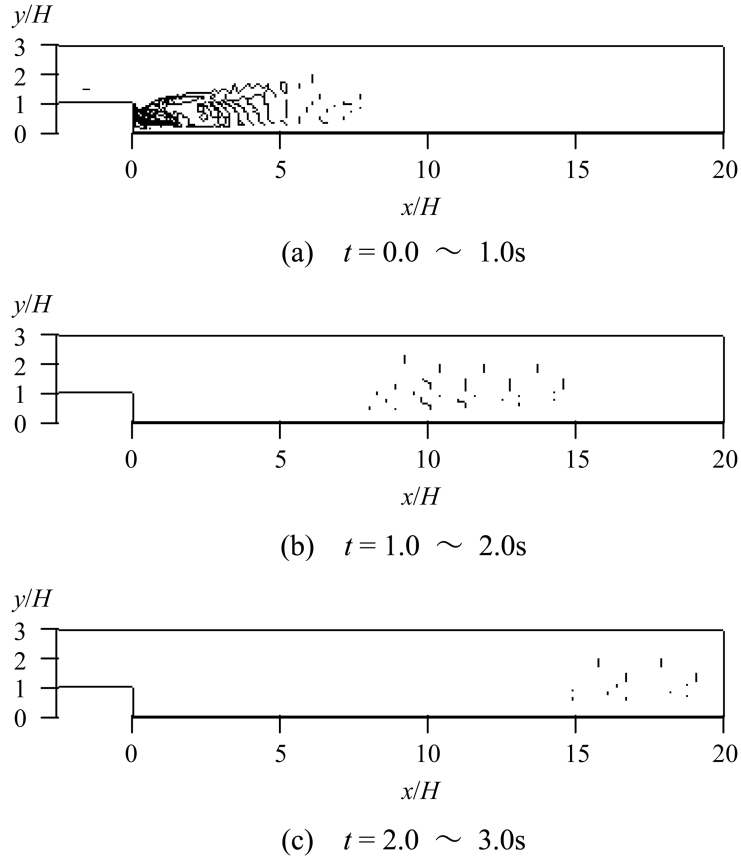


Fig. 13 Points occurred clipping to the turbulent kinetic energy during the computation by the normal form

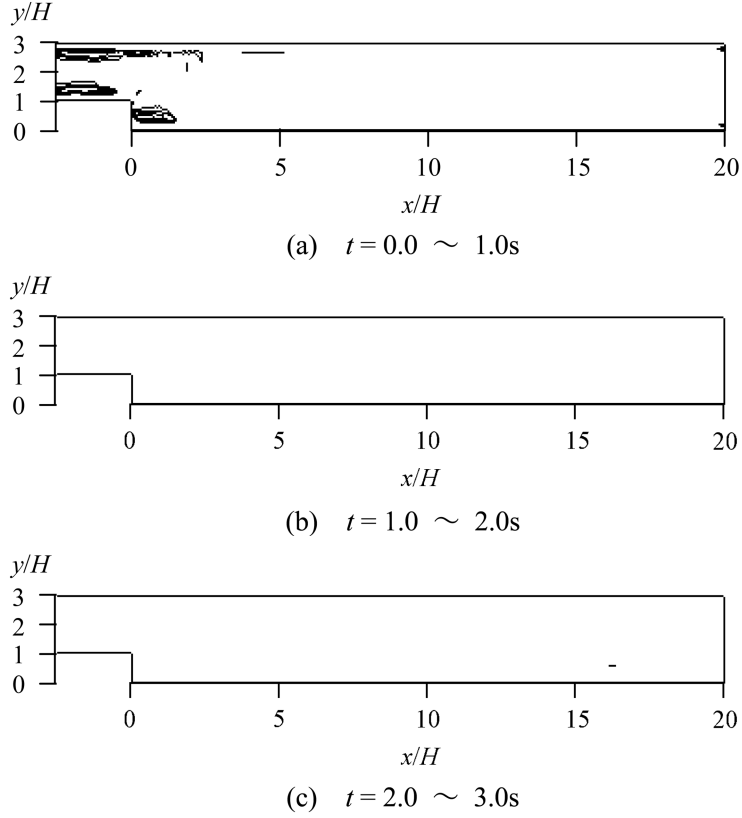


Fig. 14 Points occurred clipping to the turbulent dissipation rate during the computation by the normal form

Table 2 Specified clipping values for comparison

	$k_c$ [ $\text{cm}^2/\text{s}^2$ ]	$\varepsilon_c$ [ $\text{cm}^2/\text{s}^3$ ]
Case1	1.01	1.01
Case2	0.101	0.101
Case3	0.0101	0.0101

maximum number of clipping to  $\varepsilon$  was four times per node. As indicated in Figs. 14(b) and 14(c), clipping to  $\varepsilon$  rarely occurred from 1.0s to 2.0s and 2.0s to 3.0s. As shown in Figs. 13(b) and 13(c), the area of clipping to  $k$  moves to the downstream. The comparison of the eddy viscosity distributions in Figs. 9(a)~(c) and the motion of the clipping areas in Figs. 13 and 14 show that the clipping does not occur in the downstream of the excessive eddy viscosity. Since the eddy viscosity is a combination of  $k$  and  $\varepsilon$  as defined in Eq. (6), these results suggest strong relation between the clipping and the excessive eddy viscosity which associates with the imbalance of  $k$  and  $\varepsilon$  shown in Fig. 11.

In order to investigate the effect of the clipping further, we have changed the clipping value as listed in Table 2. Figs. 16 and 17 show the time histories of the eddy viscosity at point P1 and P2 as indicated in Fig. 15, respectively. As indicated in Fig. 17, the excessive eddy viscosities are about

one hundred larger than the value of the eddy viscosity at the steady state. On the other hands, for the logarithmic form, the excessive eddy viscosity does not occur, the maximum eddy viscosity in the transient process, as indicated in Fig. 16, is only twice as large as that of the steady state.

Although the eddy viscosities at the steady state by the normal form and by the logarithmic form become nearly same value, the excessive eddy viscosity should be avoided in the normal form. Because it may make the computation be unstable. As shown in Figs. 16 and 17, smaller clipping value reduces excessive eddy viscosity. Therefore, it may be possible to avoid the excessive eddy viscosity by using the clipping value which is very close to zero. However, it is difficult to determine

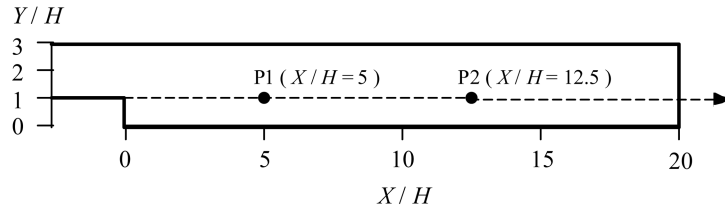


Fig. 15 Sampling points for the comparison of the clipping values

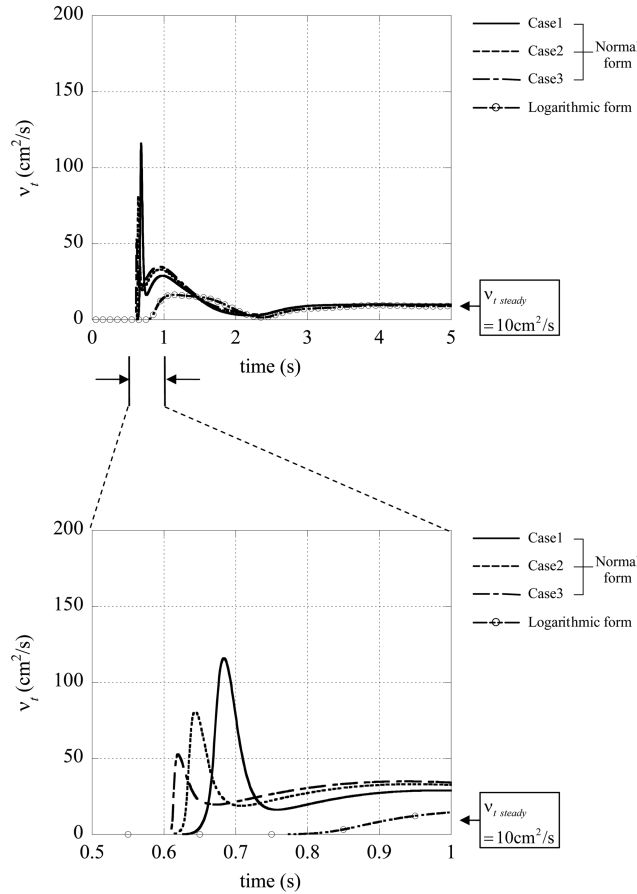


Fig. 16 Time history of the eddy viscosity at sampling point P1 in Fig.15 in three different clipping values



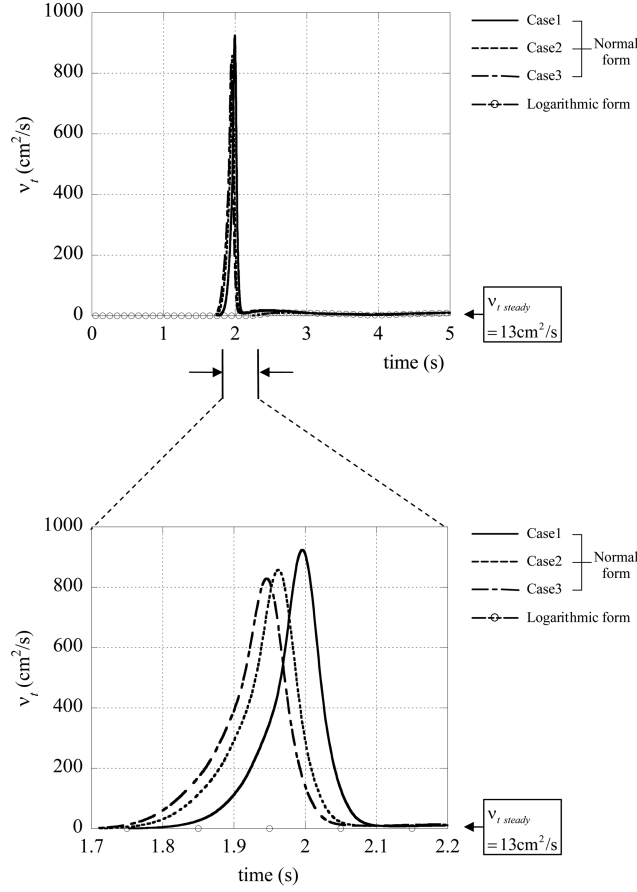


Fig. 17 Time history of the eddy viscosity at sampling point P2 in Fig.15 in three different clipping values

an appropriate clipping value a priori. Therefore, it is reasonable to employ the logarithmic form in order to achieve stable computation.

## 7. Flow around a 2D square cylinder

### 7.1. Computational conditions

In the previous example, we noticed that the logarithmic form was effective to the transient process. Therefore, we applied it to a flow around a 2D square cylinder to investigate the effect of the logarithmic form in unsteady flows. Fig. 18 shows the computational domain and the boundary conditions. On the inlet boundary, we specified that both the velocity  $\bar{U}$  and the turbulent kinetic energy  $k$  are uniform, and the eddy viscosity  $\nu_t$  is as 100 times large of the molecule viscosity  $\nu$ . The flow Reynolds number  $Re_D$  is 22,000 based on the length of the square cylinder edge  $D$  and the velocity on the inlet boundary. On the body boundary, the wall function is applied. The thickness of the modeled region by the wall function is set to  $0.03D$ . Figs. 19 and 20 show the computational meshes which has 6,378 nodes and 6,169 elements. The origin of the horizontal ( $x$ ) and the vertical ( $y$ ) coordinates is taken at the center of the square cylinder.

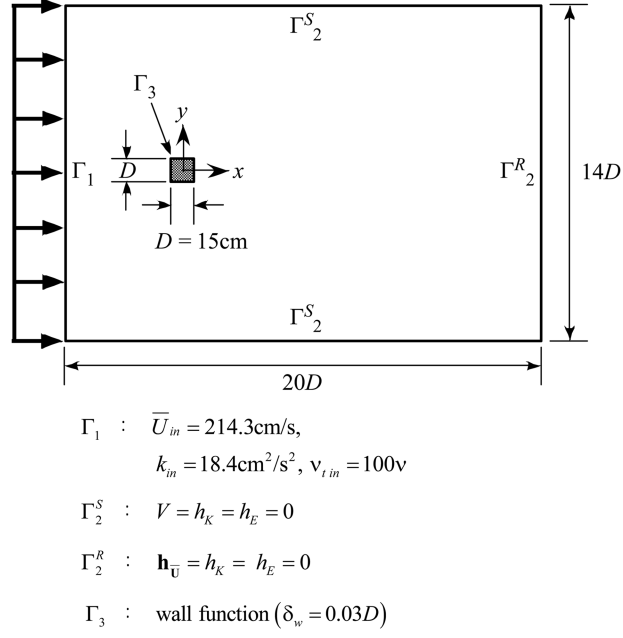


Fig. 18 Computational domain and boundary conditions

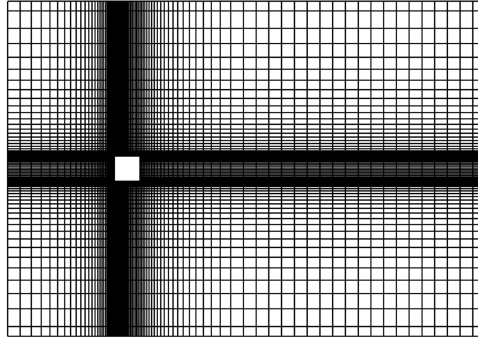


Fig. 19 Computational mesh (whole domain)

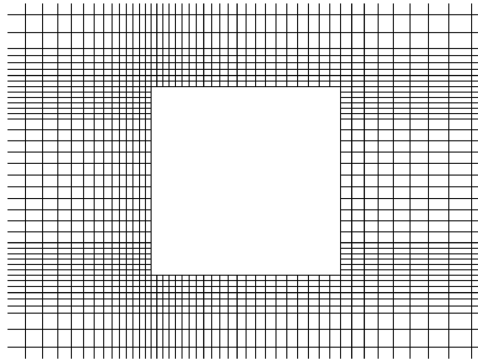
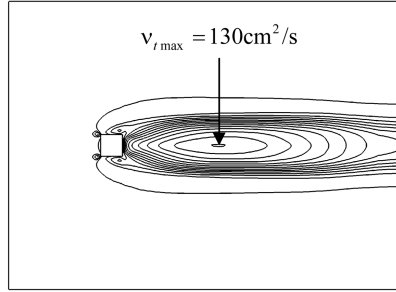


Fig. 20 Computational mesh (around the body)

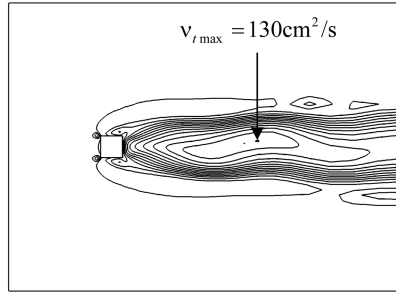
We used the modified  $k$ - $\varepsilon$  model (the Kato-Launder model) because the flow is impinging at the front face of a 2D square cylinder. The modified  $k$ - $\varepsilon$  model differs from the standard one only in the definition of the production term as given in Eqs. (10) and (11). Therefore, applying the logarithmic form to the modified  $k$ - $\varepsilon$  model, there is no difference in the computational procedures from the standard one except the production term.

## 7.2. Comparison of the normal form and the logarithmic form

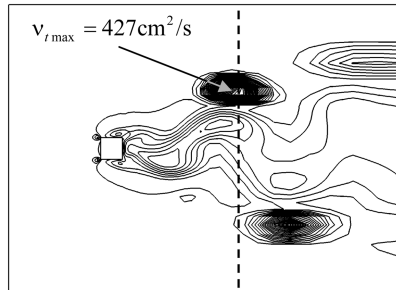
Using the normal form, the calculation became unstable and collapsed. On the other hand, the calculation by the logarithmic form didn't collapse and the solution with periodical vortex shedding was obtained. Figs. 21 and 22 show the distributions of the eddy viscosity  $\nu_t$  computed by the normal



(a) At the time instant of the symmetrical flow

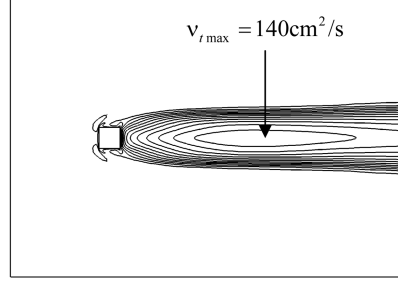


(b) At the beginning of the collapse of the symmetrical flow

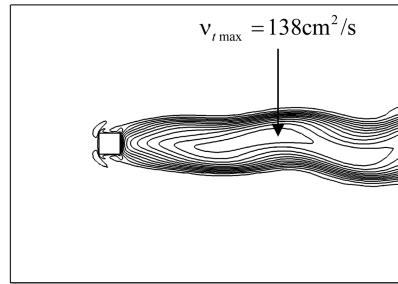


(c) Just before the occasion of the breakdown of the computation  
(The broken line indicates the cross section of the plots in Fig.23)

Fig. 21 Distribution of the eddy viscosity by the normal form at some time instants



(a) At the time instant of the symmetrical flow



(b) At the beginning of the collapse of the symmetrical flow

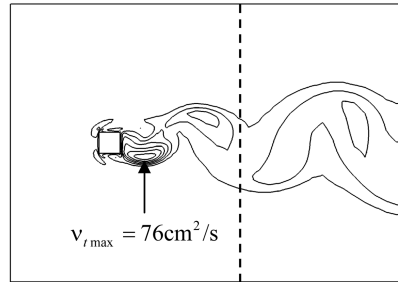
(c) At the time instant of the maximum lift force emanating  
(The broken line indicates the cross section of the plots in Fig.24)

Fig. 22 Distribution of the eddy viscosity by the logarithmic form at some time instants

form and the logarithmic form, respectively, at some time instants until the periodical vortex shedding emanating. The interval of contour line is  $10\text{cm}^2/\text{s}$ . Figs. 21(a) and 22(a) are the distributions at the time instant when the flow still keeps its symmetry. Figs. 21(b) and 22(b) are the distributions at the time instant when the flow is just losing its symmetry. Fig. 21(c) is the distribution just before the occasion of the breakdown of the computation. Fig. 22(c) is the distribution at the time instant when the maximum lift force occurs. When the flow is symmetric, there are no excessive eddy viscosities in the normal form and the logarithmic form. However, in the normal form, as the flow becomes asymmetric, excessive eddy viscosities occur at several regions where the flow is almost uniform.

Figs. 23 and 24 show the distributions of the turbulent kinetic energy  $k$ , the turbulent dissipation rate  $\varepsilon$  and the eddy viscosity  $\nu_t$  along the broken lines indicated in Figs. 21(c) and 22(c). We plotted  $k$  and  $\varepsilon$  in the logarithmic scale. As shown in Fig. 23, the eddy viscosity  $\nu_t$  computed by the normal

form is extraordinary large between  $y/D = 2$  and  $y/D = 4$  while there is no such large eddy viscosity  $\nu_t$  in the result by the logarithmic form. In this region, the turbulent dissipation rate  $\varepsilon$  becomes small locally. Therefore, the excessive eddy viscosity occurs. As is observed in the backward facing step flow, the balance between  $k$  and  $\varepsilon$  is not preserved in the normal form although it is kept in the logarithmic form. Figs. 25(a)-(d) are the distribution of the streamline, pressure, turbulent kinetic energy, and turbulent dissipation rate, respectively, at the same time instant as Fig. 22(c). For reasons mentioned above, we confirmed that the logarithmic form is effective to unsteady flows.

### 7.3. Evaluation of the coefficient of the aerodynamic forces

We evaluated the coefficient of the aerodynamic forces. Table 3 shows the mean value of the drag

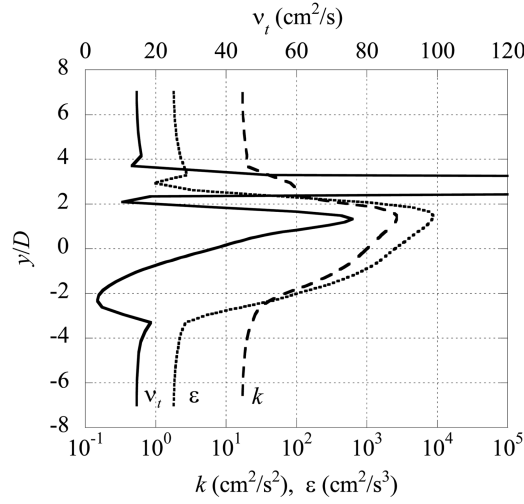


Fig. 23 Distribution of turbulent variables along the broken line in Fig. 21(c) (the result by the normal form)

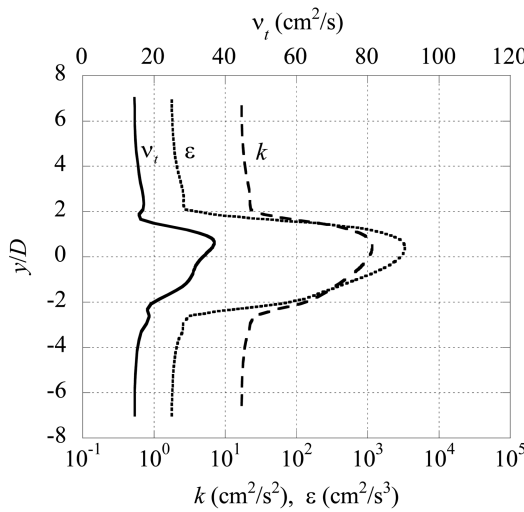


Fig. 24 Distribution of turbulent variables along the broken line in Fig. 22(c) (the result by the logarithmic form)

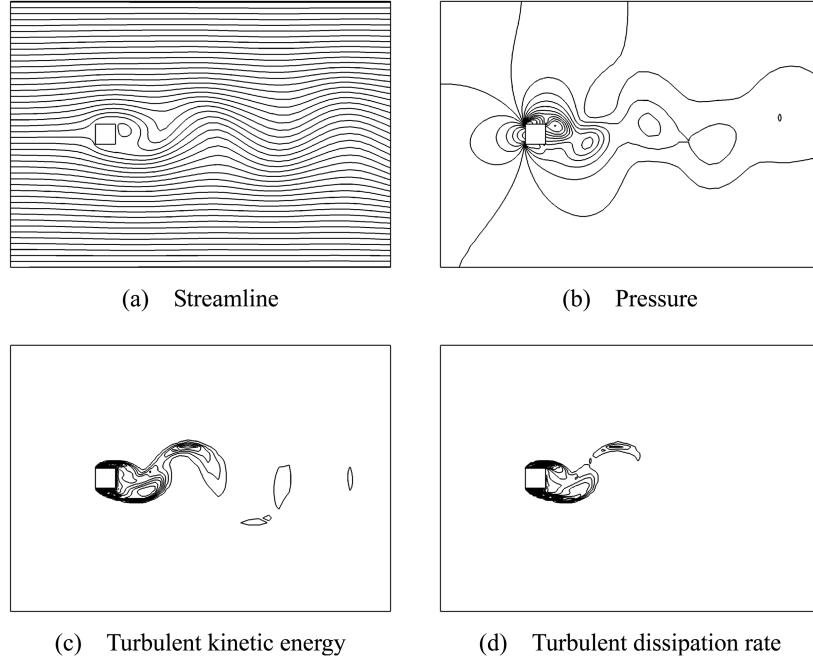


Fig. 25 Distributions at the time instant of maximum lift force arising

Table 3 Coefficients of the aerodynamic forces

	$\overline{C_D}$	$C_{L\ rms}$	$C_{L\ max}$	$S_t$
Present	2.37	0.78	1.1	0.136
Kato (Calc.)	2.05	0.82	1.2	0.145
Shimada, <i>et al.</i> (Calc.)	2.05	1.43	2.2	0.141
Kato (Exp.)	2.0 - 2.1	1.1	1.4 - 1.6	0.12 - 0.13

coefficient  $\overline{C_D}$ , the R.M.S. of the lift coefficient  $C_{L\ rms}$ , the maximum value of lift coefficient  $C_{L\ max}$  and the Strouhal number  $S_t$ . The computational and experimental results by Kato (1997) and the computational result by Shimada, *et al.* (2002) are also indicated. Although the drag coefficient is evaluated a little large in comparison with the result of Kato, there is only small difference in the lift coefficient. The lift coefficient of the present study is smaller than that of Shimada, *et al.* and closer to that of the computational work of Kato. This difference is caused by the treatment of the near wall region. Kato and we used the wall function to model the near wall region described in the section 5 while Shimada, *et al.* used the two-layer model of Rodi (1991) in which smaller eddies are resolved in the near wall region. As a result using the wall function, appropriate results are obtained in the present computation using the logarithmic form.

## 8. Conclusions

In this paper, for the numerical analysis of turbulent flows based on the  $k$ - $\varepsilon$  model, we investigated the performance of the logarithmic form proposed by Ilinca and Pelletier (1998), specially focusing on transient or unsteady flows. We calculated a flow over a backward facing step

and a flow around a 2D square cylinder. The results are summarized below.

- From the result of the backward facing step flow by the normal form, during the transient process, the clipping occurs in the region where the balance between  $k$  and  $\varepsilon$  was collapsed and consequently excessive eddy viscosity was produced locally. In addition the clipping values effects the transient process considerably.
- The use of the logarithmic form circumvented the excessive eddy viscosity and the collapse of the balance between  $k$  and  $\varepsilon$ .
- From the result of the flow around the 2D square cylinder, we find that the logarithmic form is also effective to unsteady flows.

Although the above knowledge is based on the specific time integration method and specific spatial discretization used in this study, in the analysis employed by the  $k$ - $\varepsilon$  model, the use of the logarithmic form is effective for the unsteady flow and makes the analysis stable.

## Appendix A: Explicit statement of matrices

[Momentum equation]

$$\begin{aligned}
 \mathbf{M} &= \sum_{e=1}^{N_{el}} \mathbf{M}^e = \sum_{e=1}^{N_{el}} \left[ \int_{\Omega^e} \rho \mathbf{N}_{\bar{\mathbf{u}}}^T \mathbf{N}_{\bar{\mathbf{u}}} d\Omega \right] \\
 \mathbf{A} &= \sum_{e=1}^{N_{el}} \mathbf{A}^e = \sum_{e=1}^{N_{el}} \left[ \int_{\Omega^e} \rho \mathbf{N}_{\bar{\mathbf{u}}}^T (\bar{\mathbf{U}}^T \nabla) \mathbf{N}_{\bar{\mathbf{u}}} d\Omega \right] \\
 \mathbf{D} &= \sum_{e=1}^{N_{el}} \mathbf{D}^e = \sum_{e=1}^{N_{el}} \left[ \int_{\Omega^e} \mathbf{N}_{\bar{\mathbf{u}}}^T \mathbf{L}^T \mathbf{T} \mathbf{L} \mathbf{N}_{\bar{\mathbf{u}}} d\Omega \right] \\
 \mathbf{G} &= \sum_{e=1}^{N_{el}} \mathbf{G}^e = \sum_{e=1}^{N_{el}} \left[ \int_{\Omega^e} \mathbf{N}_{\bar{\mathbf{u}}}^T \mathbf{L}^T \mathbf{m}_{\bar{p}} d\Omega \right] \\
 \mathbf{f} &= \sum_{e=1}^{N_{el}} \mathbf{f}^e = \sum_{e=1}^{N_{el}} \left[ \int_{\Omega^e} \rho \mathbf{N}_{\bar{\mathbf{u}}}^T \tilde{\mathbf{f}} d\Omega + \int_{\Gamma_h^e} \mathbf{N}_{\bar{\mathbf{u}}}^T \mathbf{h}_{\bar{\mathbf{u}}} d\Gamma \right] \\
 \tilde{\mathbf{M}} &= \sum_{e=1}^{N_{el}} \tilde{\mathbf{M}}^e = \sum_{e=1}^{N_{el}} \left[ \int_{\Omega^e} \rho \tau_{\bar{\mathbf{u}}} (\bar{\mathbf{U}}^T \nabla) \mathbf{N}_{\bar{\mathbf{u}}}^T \mathbf{N}_{\bar{\mathbf{u}}} d\Omega \right] \\
 \tilde{\mathbf{A}} &= \sum_{e=1}^{N_{el}} \tilde{\mathbf{A}}^e = \sum_{e=1}^{N_{el}} \left[ \int_{\Omega^e} \rho \tau_{\bar{\mathbf{u}}} (\bar{\mathbf{U}}^T \nabla) \mathbf{N}_{\bar{\mathbf{u}}}^T (\bar{\mathbf{U}}^T \nabla) \mathbf{N}_{\bar{\mathbf{u}}} d\Omega \right] \\
 \tilde{\mathbf{f}} &= \sum_{e=1}^{N_{el}} \tilde{\mathbf{f}}^e = \sum_{e=1}^{N_{el}} \left[ \int_{\Omega^e} \rho \tau_{\bar{\mathbf{u}}} (\bar{\mathbf{U}}^T \nabla) \mathbf{N}_{\bar{\mathbf{u}}}^T \tilde{\mathbf{f}} d\Omega \right] \\
 \mathbf{L} &= \begin{bmatrix} \partial/\partial x & 0 & \partial/\partial y \\ 0 & \partial/\partial y & \partial/\partial x \end{bmatrix}^T, \quad \mathbf{T} = (\mu + \mu_T) \begin{bmatrix} 2 & 0 & 0 \\ 0 & 2 & 0 \\ 0 & 0 & 1 \end{bmatrix}
 \end{aligned}$$

$$\mathbf{m} = \langle -1 \ -1 \ 0 \rangle^T \quad (\text{A.1})$$

[Continuity equation]

$$\mathbf{G}^T = \sum_{e=1}^{N_{el}} \mathbf{G}^T = \sum_{e=1}^{N_{el}} \left[ \int_{\Omega^e} N_{\bar{p}} \mathbf{m}^T \mathbf{L} \mathbf{N}_{\bar{u}} d\Omega \right] \quad (\text{A.2})$$

[K equation]

$$\begin{aligned} \mathbf{M}_K &= \sum_{e=1}^{N_{el}} \mathbf{M}_K^e = \sum_{e=1}^{N_{el}} \left[ \int_{\Omega^e} \mathbf{N}_K^T \mathbf{N}_K d\Omega \right] \\ \mathbf{A}_K &= \sum_{e=1}^{N_{el}} \mathbf{A}_K^e = \sum_{e=1}^{N_{el}} \left[ \int_{\Omega^e} \mathbf{N}_K^T (\bar{\mathbf{U}}^T \nabla) \mathbf{N}_K d\Omega \right] \\ \mathbf{D}_K &= \sum_{e=1}^{N_{el}} \mathbf{D}_K^e = \sum_{e=1}^{N_{el}} \left[ \int_{\Omega^e} \mathbf{N}_K^T \nabla^T \left( \mathbf{v} + \frac{\mathbf{v}_t^e}{\sigma_k} \right) \nabla \mathbf{N}_K d\Omega \right] \\ \mathbf{D}'_K &= \sum_{e=1}^{N_{el}} \mathbf{D}'_K = \sum_{e=1}^{N_{el}} \left[ \int_{\Omega^e} \mathbf{N}_K^T \left( \mathbf{v} + \frac{\mathbf{v}_t^e}{\sigma_k} \right) (\nabla K)^T \nabla \mathbf{N}_K d\Omega \right] \\ \mathbf{S}_K &= \sum_{e=1}^{N_{el}} \mathbf{S}_K^e = \sum_{e=1}^{N_{el}} \left[ \int_{\Omega^e} \mathbf{N}_K^T \mathbf{N}_K (\mathbf{P}_{PK}^e - \mathbf{P}_{NK}^e) d\Omega + \int_{\Gamma_h^e} \mathbf{N}_K \mathbf{h}_K^e d\Gamma \right] \\ \tilde{\mathbf{M}}_K &= \sum_{e=1}^{N_{el}} \tilde{\mathbf{M}}_K^e = \sum_{e=1}^{N_{el}} \left[ \int_{\Omega^e} \tau_K (\bar{\mathbf{U}}^T \nabla) \mathbf{N}_K^T \mathbf{N}_K d\Omega \right] \\ \tilde{\mathbf{A}}_K &= \sum_{e=1}^{N_{el}} \tilde{\mathbf{A}}_K^e = \sum_{e=1}^{N_{el}} \left[ \int_{\Omega^e} \tau_K (\bar{\mathbf{U}}^T \nabla) \mathbf{N}_K^T (\bar{\mathbf{U}}^T \nabla) \mathbf{N}_K d\Omega \right] \\ \tilde{\mathbf{D}}'_K &= \sum_{e=1}^{N_{el}} \tilde{\mathbf{D}}'_K = \sum_{e=1}^{N_{el}} \left[ \int_{\Omega^e} \tau_K (\bar{\mathbf{U}}^T \nabla) \mathbf{N}_K^T \left( \mathbf{v} + \frac{\mathbf{v}_t^e}{\sigma_k} \right) (\nabla K)^T \nabla \mathbf{N}_K d\Omega \right] \\ \tilde{\mathbf{S}}_K &= \sum_{e=1}^{N_{el}} \tilde{\mathbf{S}}_K^e = \sum_{e=1}^{N_{el}} \left[ \int_{\Omega^e} \tau_K (\bar{\mathbf{U}}^T \nabla) \mathbf{N}_K^T \mathbf{N}_K (\mathbf{P}_{PK}^e - \mathbf{P}_{NK}^e) d\Omega \right] \\ \mathbf{P}_{PK}^e &= \langle e^{-K_1} P_{k1}, \ e^{-K_2} P_{k2}, \ e^{-K_3} P_{k3}, \ e^{-K_4} P_{k4} \rangle^T \\ \mathbf{P}_{NK}^e &= \frac{C_{\mu}}{\mathbf{v}_t^e} \langle e^{K_1}, \ e^{K_2}, \ e^{K_3}, \ e^{K_4} \rangle^T \end{aligned} \quad (\text{A.3})$$



[ $E$  equation]

$$\begin{aligned}
\mathbf{M}_E &= \sum_{e=1}^{N_{el}} \mathbf{M}_E^e = \sum_{e=1}^{N_{el}} \left[ \int_{\Omega^e} \mathbf{N}_E^T \mathbf{N}_E d\Omega \right] \\
\mathbf{A}_E &= \sum_{e=1}^{N_{el}} \mathbf{A}_E^e = \sum_{e=1}^{N_{el}} \left[ \int_{\Omega^e} \mathbf{N}_E^T (\bar{\mathbf{U}}^T \nabla) \mathbf{N}_E d\Omega \right] \\
\mathbf{D}_E &= \sum_{e=1}^{N_{el}} \mathbf{D}_E^e = \sum_{e=1}^{N_{el}} \left[ \int_{\Omega^e} \mathbf{N}_E^T \nabla^T \left( \nu + \frac{\nu_t^e}{\sigma_\varepsilon} \right) \nabla \mathbf{N}_E d\Omega \right] \\
\mathbf{D}'_E &= \sum_{e=1}^{N_{el}} \mathbf{D}'_E^e = \sum_{e=1}^{N_{el}} \left[ \int_{\Omega^e} \mathbf{N}_E^T \left( \nu + \frac{\nu_t^e}{\sigma_\varepsilon} \right) (\nabla E)^T \nabla \mathbf{N}_E d\Omega \right] \\
\mathbf{S}_E &= \sum_{e=1}^{N_{el}} \mathbf{S}_E^e = \sum_{e=1}^{N_{el}} \left[ \int_{\Omega^e} \mathbf{N}_E^T \mathbf{N}_E (\mathbf{P}_{PE}^e - \mathbf{P}_{NE}^e) d\Omega + \int_{\Gamma_h^e} \mathbf{N}_E \mathbf{h}_E^e d\Gamma \right] \\
\tilde{\mathbf{M}}_E &= \sum_{e=1}^{N_{el}} \tilde{\mathbf{M}}_E^e = \sum_{e=1}^{N_{el}} \left[ \int_{\Omega^e} \tau_E (\bar{\mathbf{U}}^T \nabla) \mathbf{N}_E^T \mathbf{N}_E d\Omega \right] \\
\tilde{\mathbf{A}}_E &= \sum_{e=1}^{N_{el}} \tilde{\mathbf{A}}_E^e = \sum_{e=1}^{N_{el}} \left[ \int_{\Omega^e} \tau_E (\bar{\mathbf{U}}^T \nabla) \mathbf{N}_E^T (\bar{\mathbf{U}}^T \nabla) \mathbf{N}_E d\Omega \right] \\
\tilde{\mathbf{D}}'_E &= \sum_{e=1}^{N_{el}} \tilde{\mathbf{D}}'_E^e = \sum_{e=1}^{N_{el}} \left[ \int_{\Omega^e} \tau_E (\bar{\mathbf{U}}^T \nabla) \mathbf{N}_E^T \left( \nu + \frac{\nu_t^e}{\sigma_\varepsilon} \right) (\nabla E)^T \nabla \mathbf{N}_E d\Omega \right] \\
\tilde{\mathbf{S}}_E &= \sum_{e=1}^{N_{el}} \tilde{\mathbf{S}}_E^e = \sum_{e=1}^{N_{el}} \left[ \int_{\Omega^e} \tau_E (\bar{\mathbf{U}}^T \nabla) \mathbf{N}_E^T \mathbf{N}_E (\mathbf{P}_{PE}^e - \mathbf{P}_{NE}^e) d\Omega \right] \\
\mathbf{P}_{PE}^e &= C_{\varepsilon 1} \langle e^{-K_1} P_{k1}, e^{-K_2} P_{k2}, e^{-K_3} P_{k3}, e^{-K_4} P_{k4} \rangle^T \\
\mathbf{P}_{NE}^e &= C_{\varepsilon 2} \langle e^{E_1 - K_1}, e^{E_2 - K_2}, e^{E_3 - K_3}, e^{E_4 - K_4} \rangle^T
\end{aligned} \tag{A.4}$$

## Appendix B: Algorithm of the time integration

[I. Predictor phase ( $i = 0$ )]

$$\begin{cases} \dot{\mathbf{u}}_{n+1}^{(0)} = \mathbf{0} \\ \mathbf{u}_{n+1}^{(0)} = \mathbf{u}_n + (1 - \theta) \Delta t \dot{\mathbf{u}}_n \\ \mathbf{p}_{n+1}^{(0)} = \mathbf{p}_n \end{cases}$$

$$\begin{cases} \dot{\mathbf{K}}_{n+1}^{(0)} = \mathbf{0} \\ \mathbf{K}_{n+1}^{(0)} = \mathbf{K}_n + (1 - \theta) \Delta t \dot{\mathbf{K}}_n \end{cases}$$

$$\begin{cases} \dot{\mathbf{E}}_{n+1}^{(0)} = \mathbf{0} \\ \mathbf{E}_{n+1}^{(0)} = \mathbf{E}_n + (1 - \theta)\Delta t \dot{\mathbf{E}}_n \end{cases}$$

\* Update  $\tau_w, P_k, \varepsilon, \varepsilon_p$  on the wall boundary nodes by the wall function

(B.1)

[II. Solution phase ( $i = 1, 2$ )]

$$\begin{cases} \mathbf{M}_L \Delta \dot{\mathbf{u}}^{*(i)} = \mathbf{f} - \mathbf{M} \dot{\mathbf{u}}_{n+1}^{(i)} - \mathbf{N}(\mathbf{u}_{n+1}^{(i)}) \mathbf{u}_{n+1}^{(i)} - \mathbf{D} \mathbf{u}_{n+1}^{(i)} + \mathbf{G} \mathbf{p}_{n+1}^{(i)} \\ \mathbf{u}^{*(i)} = \mathbf{u}_{n+1}^{(i)} + \theta \Delta t \Delta \dot{\mathbf{u}}^{*(i)} \\ \{\mathbf{G}^T (\mathbf{M}_L)^{-1} \mathbf{G}\} \Delta \mathbf{p}^{(i)} = \mathbf{G}^T \mathbf{u}^{*(i)} / \theta \Delta t \\ \Delta \dot{\mathbf{u}}_{n+1}^{(i)} = \Delta \dot{\mathbf{u}}^{*(i)} + (\mathbf{M}_L)^{-1} \mathbf{G} \Delta \mathbf{p}^{(i)} \end{cases}$$

$$\begin{cases} \mathbf{M}_L^K \Delta \dot{\mathbf{K}}_{n+1}^{(i)} = \mathbf{S}^K - \mathbf{M}^K \dot{\mathbf{K}}_{n+1}^{(i)} - \mathbf{N}^K(\mathbf{u}_{n+1}^{(i)}) \mathbf{K}_{n+1}^{(i)} \\ \quad - \mathbf{D}^K \mathbf{K}_{n+1}^{(i)} + \tilde{\mathbf{D}}^K(\mathbf{K}_{n+1}) \mathbf{K}_{n+1}^{(i)} \\ \mathbf{M}_L^E \Delta \dot{\mathbf{E}}_{n+1}^{(i)} = \mathbf{S}^E - \mathbf{M}^E \dot{\mathbf{E}}_{n+1}^{(i)} - \mathbf{N}^E(\mathbf{u}_{n+1}^{(i)}) \mathbf{E}_{n+1}^{(i)} \\ \quad - \mathbf{D}^E \mathbf{E}_{n+1}^{(i)} + \tilde{\mathbf{D}}^E(\mathbf{E}_{n+1}) \mathbf{E}_{n+1}^{(i)} \end{cases}$$

(B.2)

[ III. Corrector Phase (  $i = 1, 2$  ) ]

$$\begin{cases} \dot{\mathbf{u}}_{n+1}^{(i)} = \dot{\mathbf{u}}_{n+1}^{(i)} + \Delta \dot{\mathbf{u}}_{n+1}^{(i)} \\ \mathbf{u}_{n+1}^{(i)} = \mathbf{u}_{n+1}^{(i)} + \theta \Delta t \Delta \dot{\mathbf{u}}_{n+1}^{(i)} \\ \mathbf{p}_{n+1}^{(i)} = \mathbf{p}_{n+1}^{(i)} + \Delta \mathbf{p}^{(i)} \end{cases}$$

$$\begin{cases} \dot{\mathbf{K}}_{n+1}^{(i)} = \dot{\mathbf{K}}_{n+1}^{(i)} + \Delta \dot{\mathbf{K}}_{n+1}^{(i)} \\ \mathbf{K}_{n+1}^{(i)} = \mathbf{K}_{n+1}^{(i)} + \theta \Delta t \Delta \dot{\mathbf{K}}_{n+1}^{(i)} \end{cases}$$

$$\begin{cases} \dot{\mathbf{E}}_{n+1}^{(i)} = \dot{\mathbf{E}}_{n+1}^{(i)} + \Delta \dot{\mathbf{E}}_{n+1}^{(i)} \\ \mathbf{E}_{n+1}^{(i)} = \mathbf{E}_{n+1}^{(i)} + \theta \Delta t \Delta \dot{\mathbf{E}}_{n+1}^{(i)} \end{cases}$$

\* Update  $\tau_w, P_k, \varepsilon, \varepsilon_p$  on the wall boundary nodes by the wall function

(B.3)

## References

Abe, K., Jang, Y.J. and Leschziner, M. A. (2003), "An investigation of wall-anisotropy expressions and length-scale equations for non-linear eddy-viscosity models", *Int. J. Heat Fluid Fl.*, **24**, 181-198.

- Abe, K., Nagano, Y. and Kondoh, T. (1992), "An improved  $k$ - $\epsilon$  model for prediction of turbulent flows with separation and reattachment", *JSME J., Part B*, **58-554**, 3003-3010 (in Japanese).
- Bauer, W., Haag, O. and Hennecke, D. K. (2000), "Accuracy and robustness of nonlinear eddy viscosity models", *Int. J. Heat Fluid Fl.*, **21**, 312-319.
- Brooks, A.N. and Hughes, T.J.R. (1982), "Streamline upwind / Petrov-Galerkin formulations for convection dominated flows with particular emphasis on the incompressible Navier-Stokes equations", *Comput. Methods Appl. M.*, **32**, 199-259.
- Craft, T. J., Launder, B. E. and Suga, K. (1996), "Development and application of a cubic eddy-viscosity model of turbulence", *Int. J. Heat Fluid Fl.*, **17**, 108-115.
- Ferziger, J.H. , Kline, S.J. , Avva, R.K., Bordalo, S.N. and Tzuoo, K.L. (1990), "Zonal Modeling of Turbulent Flows - Philosophy and Accomplishments", *Near-Wall Turbulence*, 800-817.
- Ilinca, F. , Hetu, J.F. and Pelletier, D. (1998), "A unified finite element algorithm for two equation models of turbulence", *Comput. Fluids*, **27**(3), 291-300.
- Ilinca, F. and Pelletier, D. (1998), "Positivity Preservation and Adaptive Solution for the  $k$ - $\epsilon$  Model of Turbulence", *AIAA J.*, **36**(1), 44-50.
- Ignat, L. , Pelletier, D. and Ilinca, F. (2000), "A universal formulation of two-equation models for adaptive computation of turbulent flows", *Comput. Methods Appl. M.*, **189**, 1119-1139.
- Jones, W. P. and Launder, B. E. (1972), "The prediction of laminarization with a two-equation model of turbulence", *Int. J. Heat Mass Tran.*, **15**, 301-314.
- Kasagi, N. and Matsunaga, A. (1994), "Three-dimensional particle-tracking velocimetry measurement of turbulence statics and energy budget in a backward-facing step flow", *Int. J. Heat Fluid Fl.*, **16**, 477-485.
- Kato, M. (1997), "2-D turbulent flow analysis with modified  $k$ - $\epsilon$  around a stationary square cylinder and vibrating one in the along and across wind", *J. Struct. Mech. Earthquake Eng.*, JSCE, **577**(I-41), 217-230 (in Japanese).
- Lacasse, D., Turgeon, E. and Pelletier, D. (2001), "Prediction of turbulent separated flow in a turnaround duct using wall functions and adaptivity", *Int. J. Comput. Fluid D.*, **15**, 209-225.
- Lacasse, D., Turgeon, E. and Pelletier, D. (2004), "On the judicious use of the  $k$ - $\epsilon$  model, wall functions and adaptivity", *Int. J. Therm. Sci.*, **43**, 925-938.
- Lardeau, S. and Leschziner, M. A. (2005), "Unsteady RANS modeling of wake-blade interaction: computational requirements and limitations", *Comput. Fluids*, **34**, 3-21.
- Launder, B. E. and Spalding, D. B. (1974), "The numerical computation of turbulent flows", *Comput. Methods Appl. M.*, **3**, 269-289.
- Le, H., Moin, P. and Kim, J. (1997), "Direct numerical simulation of turbulent flow over a backward-facing step", *J. Fluid Mech.*, **330**, 349-374.
- Luo, H., Baum, J. D. and Lohner, R. (2003), "Computation of compressible flows using a two-equation turbulence model on unstructured grids", *Int. J. Comput. Fluid D.*, **17**, 87-93.
- Maurizi, A., Palma, J. M. L. M. and Castro, F. A. (1998), "Numerical simulation of the atmospheric flow in a mountainous region of the North Portugal", *J. Wind Eng. Ind. Aerod.*, **74-76**, 219-228.
- Mohammadi, B. and Pironneau, O. (1994), "Analysis of the K-Epsilon turbulence model", Masson.
- Mohammadi, B. and Puigt, G. (2006), "Wall functions in computational fluid mechanics", *Comput. Fluids*, **35**, 1108-1115.
- Rodi, W. (1991), "Experience with two-layer models combining the  $k$ - $\epsilon$  model with a one-equation model near the wall", *AIAA paper* 91-0216.
- Shimada, K. and Ishihara, T. (2002), "Application of a modified  $k$ - $\epsilon$  model to the prediction of aerodynamic characteristics of rectangular cross-section cylinders", *J. Fluids Struct.*, **16**(4), 465-485.
- Turgeon, E., Pelletier, D. and Ignat, L. (2000), "Effects of adaptivity on finite element schemes for turbulent heat transfer and flow predictions", *Numer. Heat Tr: A-Appl.*, **38**, 847-868.
- Yamaguchi, A., Ishihara, T. and Fujino, Y. (2003), "Experimental study of the wind flow in a coastal region of Japan", *J. Wind Eng. Ind. Aerod.*, **91**, 247-264.
- Yoshie, R., Mochida, A. Tominaga, Y., Kataoka, H., Harimoto, K., Nozu, T. and Shirasawa, T. (2007), "Cooperative project for CFD prediction of pedestrian wind environment in the Architectural Institute of Japan", *J. Wind Eng. Ind. Aerod.*, **95**, 1551-1578.